PCCP

ROYAL SOCIETY OF CHEMISTRY

PAPER

View Article Online
View Journal

Cite this: DOI: 10.1039/c9cp05833h

Effect of electrostatic interaction on the leaflet-specific diffusion in a supported lipid bilayer revealed by fluorescence lifetime correlation analysis†

Takuhiro Otosu and Shoichi Yamaguchi*

Received 28th October 2019,
Accepted 11th December 2019

DOI: 10.1039/c9cp05833h

rsc.li/pccp

A supported lipid bilayer (SLB) is now an indispensable tool to analyze the dynamical properties of biomembranes. However, the effect of a solid support on the leaflet-specific lipid dynamics in a SLB remains elusive, which hampers the further application of the SLB as a model biomembrane. Here, we performed the leaflet-specific lipid diffusion analysis by means of two-dimensional fluorescence lifetime correlation spectroscopy to elucidate the effect of the electrostatic interaction between lipid headgroups and a glass surface on the lipid diffusion in each leaflet of the SLB. The results clearly showed the correlation between the strength of the electrostatic interaction and the lipid diffusion in the proximal leaflet of the SLB facing a glass surface. In particular, the electrostatic attraction between the cationic lipids and a negatively charged glass surface enhanced the lipid diffusion in the proximal leaflet of the SLB, providing important implications for the lipid dynamics not only in the SLB but also in biomembranes.

Introduction

A biological membrane (or biomembrane) is a unique functional membrane that works as a functional barrier.[1] A biomembrane is composed of a lipid bilayer, and the hydrophobic moiety of lipids in the bilayer prevents many hydrophilic molecules and ions from passing through the membrane. On the other hand, the selective transportation of such molecules through the membrane is achieved *via* various transmembrane proteins embedded on the lipid bilayer, which is crucial for signal transduction,[2] generation of membrane potential,[3] ATP synthesis,[4] and so on. Extensive studies have shown that the fluidity of the membranes and the transient formation of functional microdomains (“lipid raft”) are important for the unique biological functions of biomembranes.[5–7] Because the fluidity of biomembranes is mainly governed by the dynamical properties of the lipid bilayer, understanding the lipid dynamics in the bilayer is prerequisite for elucidating the biological functions of biomembranes.

A supported lipid bilayer (SLB) is a model biomembrane formed on a solid substrate.[8–11] Because the membrane is supported by a solid substrate such as mica and silica, the SLB has high stability as compared to other model biomembranes, *e.g.*, a freestanding bilayer and a giant unilamellar vesicle. In addition, the SLB is fluidic due to the presence of a thin water layer between lipids and a support, which enables us to analyze the dynamical properties of lipid membranes through the SLB, *e.g.*, lipid diffusion,[12,13] flip-flop,[14,15] microdomain formation,[16–18] and so on.

However, it is still an open question of how the lipid dynamics in a SLB is affected by the presence of solid supports. Because the lipid–support interaction is expected to be modulated by the electrostatic interaction between the lipid headgroups and the surface charge of the supports, extensive studies have been done to elucidate the effect of ionic strength, pH and the charge of lipid headgroups on the dynamical/conformational properties of the SLB as well as the SLB formation process.[12,19–26] For instance, Cremer and Boxer have systematically examined the spreading of glass-supported SLBs as functions of pH and ionic strength of the surrounding solvent.[19] Their data showed that neither anionic nor cationic SLBs show the spreading at high pH where the glass surface is negatively charged, which allowed them to conclude that the electrostatic interaction is not responsible for the SLB spreading. On the other hand, Kataoka-Hamai and Higuchi have performed diffusion analysis of lipids in cationic and zwitterionic SLBs at various pHs.[12] Their results showed that the diffusion coefficient of a cationic SLB is sensitive to pH whereas that of a zwitterionic SLB is insensitive, suggesting the

Department of Applied Chemistry, Graduate School of Science and Engineering, Saitama University, 255 Shimo-Okubo, Sakura, Saitama 338-8570, Japan

† Electronic supplementary information (ESI) available: Precise description of 2D FLCS and FLCS, and Fig. S1–S7. See DOI: 10.1039/c9cp05833h

importance of the electrostatic interaction between the lipid headgroups and solid supports. Thus, the effect of electrostatic interaction between the lipid headgroup and a glass surface on the lipid diffusion of the SLB needs further clarification.

Two-dimensional fluorescence lifetime correlation spectroscopy (2D FLCS) is a novel single-molecule technique that enables us to analyze the inhomogeneity of the system and its dynamics through the correlation of fluorescence lifetime with the high time resolution beyond the ordinary single-molecule techniques.[27–30] Previous works have revealed the applicability of 2D FLCS to elucidate the microsecond conformational dynamics of proteins as well as DNA.[29,31–33] Because 2D FLCS is the extension of fluorescence correlation spectroscopy, this technique is also utilized to analyze the diffusion dynamics of multiple species simultaneously in a species-specific manner. This advantage is beneficial to elucidate the diffusion of lipids in a SLB in a leaflet-specific way. We very recently applied 2D FLCS to analyze the leaflet-specific lipid diffusion in a SLB.[34,35] Potassium iodide was utilized to selectively quench the fluorescence of head-labelled lipids in the distal leaflet of the SLB facing bulk solution. This enables us to statistically separate the detected signals into those of the proximal and distal leaflets through the difference in their fluorescence lifetimes induced by the iodide ions. The data clearly showed that the lipid diffusion in the proximal leaflet of a zwitterionic SLB depends on the surface charge density of a glass support whereas that in the distal one is unchanged, strongly suggesting that the interleaflet interaction is weak in the lipid bilayer of monounsaturated lipids. Because most of the previous studies have investigated the lipid dynamics in a SLB as an average of both leaflets, the leaflet-specific lipid diffusion analysis by 2D FLCS is expected to give important implications on the effect of solid supports on the lipid dynamics in a SLB.

Here, we investigated the effect of lipid headgroups on the leaflet-specific lipid diffusion of glass-supported SLBs. Because a glass surface possesses a negative charge whose density depends on pH, it is expected that the electrostatic interaction between a SLB and the glass surface depends on the net charge of the lipid headgroups as well as pH. The leaflet-specific lipid diffusion analyses by 2D FLCS clearly revealed the correlation between the strength of lipid–glass electrostatic interaction and the lipid diffusion in the proximal leaflet of a SLB. In particular, the result of the cationic SLB showed that the strong electrostatic attraction between the lipid headgroup and a glass surface enhances the lipid diffusion in the proximal leaflet of the SLB.

Experimental methods

Materials

1,2-Dioleoyl-*sn*-glycero-3-phosphocholine (DOPC), 1,2-dioleoyl-3-trimethylammonium propane (DOTAP) and 1,2-dioleoyl-*sn*-glycero-3-phospho-L-serine (DOPS) were purchased from Avanti Polar Lipids (Fig. 1), and (tetramethylrhodamine-6-thiocarbamoyl)-1,2-dihexadecanoyl-*sn*-glycero-3-phosphoethanolamine (TRITC-DHPE) was purchased from Biotium. All other reagents were of analytical grade and used without further purification.

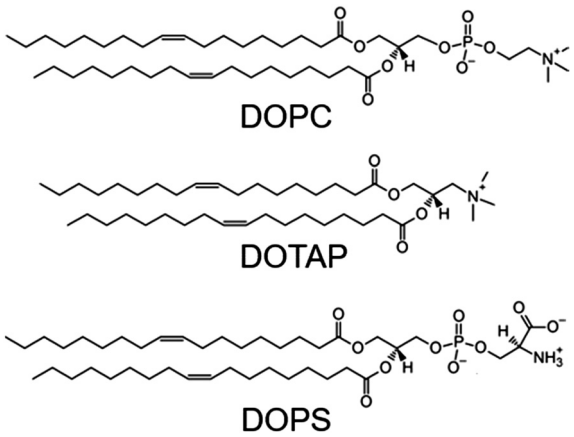

Fig. 1 Chemical structures of DOPC, DOTAP and DOPS.

Preparation of supported lipid bilayers

SLBs with different lipid compositions were formed on a cleaned glass coverslip (Thorlabs) by a vesicle fusion method as described in the literature.[36] Briefly, a lipid mixture in chloroform was prepared in a glass vial, and chloroform was evaporated under low pressure for more than 3 h. The final concentration of fluorescent lipids was set to $\sim 1.6 \times 10^{-4}$ mol%. After that, the lipid film was suspended with buffer solution, and the suspension was subjected to extrusion by using a polycarbonate filter (Avanti Polar Lipids, pore size ϕ = 100 nm) to form large unilamellar vesicles (LUVs). The following 20 mM buffers were used depending on pH: pH 5.0; acetate buffer, pH 6.4, 6.5 and 7.0; HEPES buffer, pH 7.5, 8.0 and 8.5; Tris buffer, pH 10.0; glycine buffer. Each buffer contained 100 mM NaCl and 1 mM $CaCl_2$. LUV solution was then pipetted onto a glass coverslip that was precleaned by using piranha solution. After the 30 min incubation, unreacted LUVs were removed by exchanging the solution with the corresponding buffer solution. Potassium iodide (KI) in the buffer was then gently applied to the solution above the SLB. The final concentration of KI was set to 50 mM. Measurements were started after the 20 min incubation.

2D FLCS and FLCS

Photon data from SLBs were measured by using a home-made total internal reflection (TIR) microscope system that incorporates a picosecond diode laser (BDL-510-SMN, Becker & Hickl GmbH) and a time-correlated single-photon counting (TCSPC) board (SPC-130EM, Becker & Hickl GmbH). Precise description of the instrument is found in the literature.[37] Briefly, excitation pulses from the laser enter the periphery of a TIR objective (CFI Apo TIRF, 60×, NA 1.49, NIKON), and emitted fluorescence photons from SLBs are collected with the same objective. The collected photons are passed through a dichroic mirror (ZT532rdc, Chroma Technology), a long-pass filter (ET 542lp. Chroma Technology) and a bandpass filter (ET575/50m, Chroma Technology)

before being detected by a single-photon avalanche photodiode (SPD-050-CTE-FC, Micro Photon Devices). The detected signals from the photodiode are then sent to a TCSPC board. Temporal information is recorded for all detected photons, that is, macrotime and microtime. Macrotime (T) is an absolute detection time of fluorescence photons from the start of the experiment, and microtime (t) is an excitation–emission delay time (Fig. S1, ESI†). This information is used for 2D FLCS and FLCS analyses.

In 2D FLCS, a two-dimensional emission-delay (microtime) correlation map is constructed from the photon data.[27] In the map, horizontal and vertical axes correspond to the t of 1st photons and 2nd photons, respectively, the latter of which are measured with a certain macrotime-delay time (ΔT) from the 1st photons. After subtracting the uncorrelated photons from the map, two-dimensional maximum entropy method (2D MEM) analysis is performed on the map to extract the number and lifetime distributions of all independent lifetime species. The independent fluorescence decay curves are then obtained by performing Laplace transform on the corresponding lifetime distributions. This enables us to extract the correct fluorescence decay curves of all independent lifetime species in a model-free manner.[28,29]

The independent fluorescence decay curves and the ensemble-averaged fluorescence decay curves (microtime histogram) calculated from the same photon data are then used in FLCS analysis developed by the Enderlein group.[38] In FLCS, one calculates the filter values ($f_i^{(k)}$) of each independent species (k) as a function of the microtime channel (i).[38–40] These values are used for the calculation of species-specific autocorrelation as well as cross-correlation curves as follows:

$$G^{(kl)}(\Delta T) = \frac{\left\langle \sum_i f_i^{(k)} I_i(T) \sum_j f_j^{(l)} I_j(T+\Delta T) \right\rangle}{\left\langle \sum_i f_i^{(k)} I_i(T) \right\rangle \left\langle \sum_j f_j^{(l)} I_j(T) \right\rangle}. \quad (1)$$

The calculated G represents the autocorrelation when $k = l$, and the data describe the cross-correlation when $k \neq l$. Details of 2D FLCS and FLCS analyses as well as the leaflet-specific lipid diffusion analysis performed in this study are found in the ESI† as well as the literature.[28,29,35,38–40]

Results and discussion

Fig. 2 shows the ensemble-averaged fluorescence decay curves of fluorescent lipids in various SLBs with different concentrations of a cationic lipid, DOTAP. Data were measured at pH 10.0 in the presence of KI in the bulk phase above the SLBs. Because a fluorescent lipid (TRITC-DHPE) is headgroup-labelled, the fluorescence from the lipids in the distal leaflet of SLBs facing bulk solution is selectively quenched by the iodide ions, and its lifetime becomes shorter than that in the proximal leaflet facing a glass surface. The fluorescence decay curve becomes shorter by increasing the relative concentration of DOTAP. This indicates that the fluorescent lipids are preferentially populated in the distal leaflet of the SLB in the presence of DOTAP.

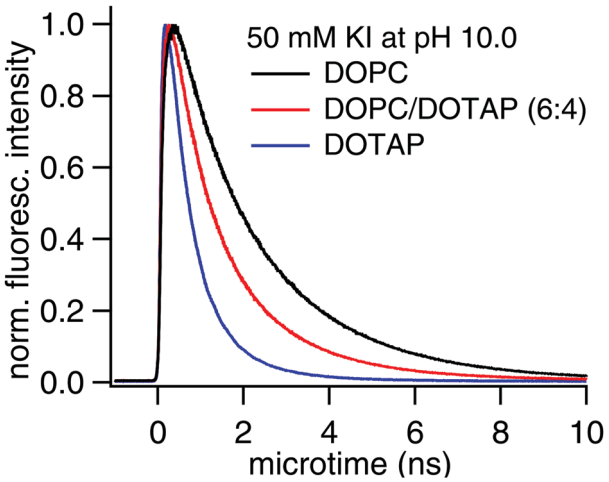

Fig. 2 Fluorescence decay curves of fluorescent lipids in a supported DOPC bilayer (black), a supported DOPC/DOTAP bilayer (red) and a supported DOTAP bilayer (blue) measured at pH 10.0. The weight percentage of DOTAP is 40% in a supported DOPC/DOTAP bilayer. Data were measured in the presence of potassium iodide. Data were normalized at the maximum intensity.

In other words, the data suggest that DOTAP populates in the proximal leaflet of the SLB and expels the fluorescent lipids from the proximal side to the distal side. It is expected that the fluorescent lipids, DOTAP, and DOPC are equally distributed in both leaflets when these lipids form LUVs. Thus, this result suggests that the distribution of the lipids changes during vesicle fusion and/or subsequent SLB formation processes probably due to the electrostatic attraction between a negatively charged glass surface and DOTAP. Based on the results shown in Fig. 2, we chose the supported DOPC/DOTAP bilayer (DOPC/DOTAP SLB) with a DOPC : DOTAP weight ratio of 6 : 4, where the contribution from the proximal leaflet having longer fluorescence lifetime is sufficiently observed in the corresponding fluorescence decay curve.

Fig. 3 shows representative two-dimensional (2D) emission-delay correlation maps of the DOPC/DOTAP SLB calculated at macrotime delay times (ΔTs) of ΔT = 100–180 μs and 300–400 μs. The data measured at pH 5.0 and 10.0 are shown. These maps describe the correlation of microtime between 1st and 2nd photons. A global 2D maximum entropy method (MEM) analysis was performed on these maps to extract the independent fluorescence decay curves. Two independent species are found in all photon data measured at various pH. Because the fluorescence decay curve of longer lifetime species shown in blue in Fig. 3c and f is almost identical to that of the ensemble-averaged one in the absence of KI, the species can be assigned to the fluorescent lipids in the proximal leaflet of the SLB. The shorter lifetime species then corresponds to that in the distal one as previously assigned in the case of the DOPC SLB.[35]

Fig. 4 shows the correlated fluorescence decay curves of fluorescent lipids in the DOPC/DOTAP SLB calculated at ΔT = 300–400 μs and 100–101 ms. The data measured at pH 5.0 and pH 10.0 are shown in Fig. 4a and b, respectively. The correlated

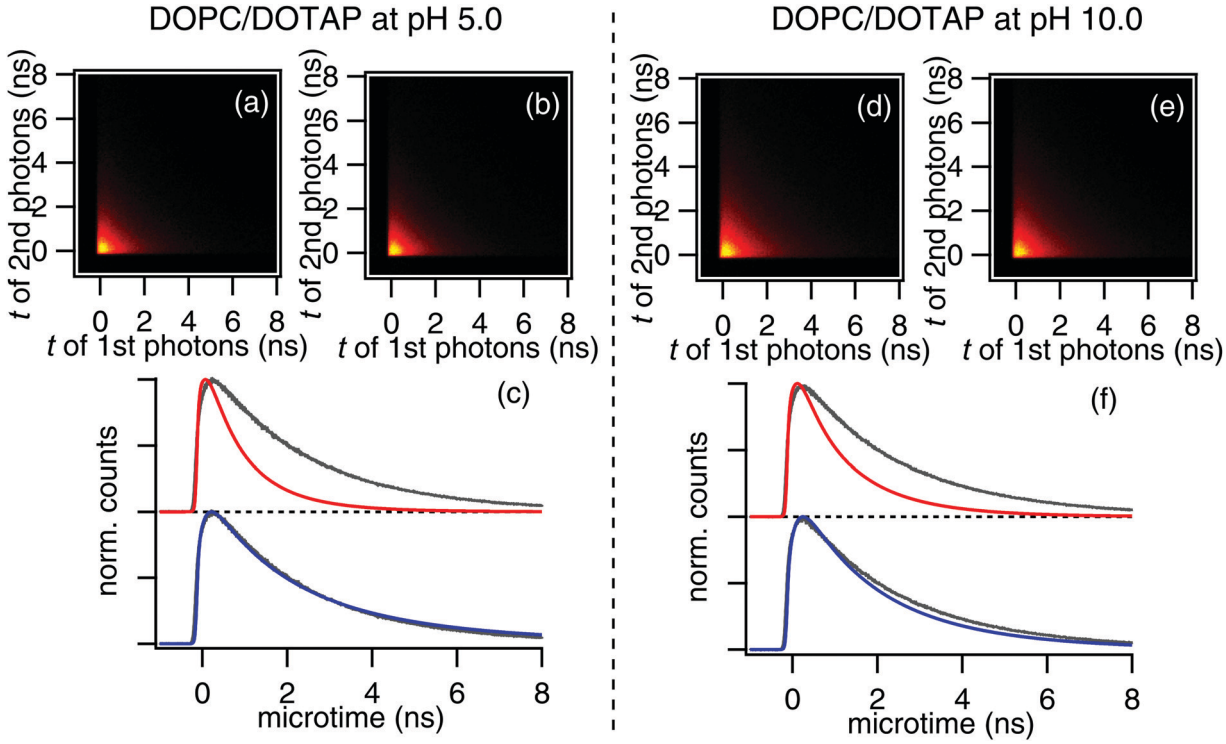

Fig. 3 Two-dimensional (2D) emission-delay correlation maps (a, b, d and e) and the independent fluorescence decay curves (c and f) of fluorescent lipids in a supported DOPC/DOTAP bilayer measured at pH 5.0 (a–c) and 10.0 (d–f). The maps were calculated with the macrotime delays of ΔT = 100–180 (a and d) and 300–400 μs (b and e). The independent fluorescence decay curves were calculated by performing a global 2D maximum entropy method analysis on these 2D maps. For comparison, the ensemble-averaged fluorescence decay curve of fluorescent lipids in the absence of potassium iodide is shown with a gray solid line.

fluorescence decay curves are calculated by integrating the corresponding 2D emission-delay correlation maps along the 2nd photon axis. The ordinary fluorescence intensity–correlation curve decays with a time constant of ~0.1 s (Fig. S2, ESI†), so that the data at smaller and larger ΔTs correspond to the flat and slope regions of the correlation curve, respectively. When two species with different fluorescence lifetimes exist in the system, the correlated decay curve at smaller ΔT shows both contributions. On the other hand, the decay curve at larger ΔT can be different from that at smaller ΔT when one of the species diffuses faster than the other. It is because the contribution of two species to the correlated photons changes due to the diffusion difference. Therefore, comparison of the two correlated decay curves gives us information about how different the diffusions of two independent lifetime species are.

The data at pH 5.0 show that the correlated decay curve at ΔT = 100–101 ms decays slower than that calculated at ΔT = 300–400 μs. This indicates that the contribution of shorter lifetime species becomes smaller with increasing ΔT, suggesting that the shorter lifetime species corresponding to the lipids in the distal leaflet diffuses faster than the lipids in the proximal one having the longer fluorescence lifetime. The same trend was previously observed in the DOPC SLB at the same pH.[35] On the other hand, the correlated decay curve at larger ΔT decays faster than that at smaller ΔT at pH 10.0. This observation is different from that of the DOPC SLB, where the correlated decay curves at this pH are almost identical irrespective of ΔT.[35] This suggests that the lipids in the proximal leaflet of the DOPC/DOTAP SLB diffuse faster than those in the distal one at pH 10.0.

To quantitatively analyze the ΔT-dependent change in the contribution of each species to the correlation curves, pH- and leaflet-specific correlation curves are calculated by means of 2D FLCS and FLCS. Fig. 5 shows the leaflet-specific autocorrelation curves of fluorescent lipids in the DOPC/DOTAP SLB at various pHs. Filter values used for the calculation and the corresponding cross-correlation curves are shown in Fig. S3 and S4 (ESI†), respectively. The cross-correlation shows unity at all ΔT regions irrespective of pH, indicating that the exchange of fluorescent lipids between the proximal and distal leaflets, that is, flip-flop, is much slower than ~1 s.

At low pH, the correlation curve of lipids in the proximal leaflet of the SLB decays slower than that in the distal one, suggesting that the diffusion of lipids in the proximal leaflet is slower than that in the distal one as expected from the comparison of the correlated decay curves shown in Fig. 4a. This observation is also in line with the results of the DOPC SLB.[35] Remarkably, the leaflet-specific autocorrelation curves at high pH show that the correlation curve of lipids in the proximal leaflet decays faster than that in the distal one. This observation is different from the results of the DOPC SLB, where the correlation curves of both leaflets are identical.[35] This indicates that the lipid diffusion in the proximal leaflet of the DOPC/DOTAP SLB is faster than that in the distal leaflet

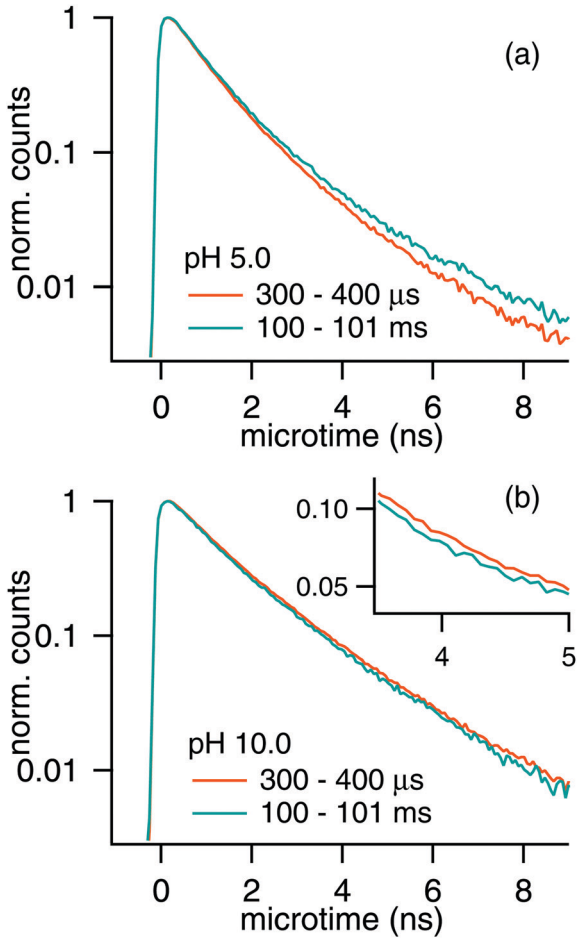

Fig. 4 Correlated fluorescence decay curves of fluorescent lipids in a supported DOPC/DOTAP bilayer at the macrotime delay time of ΔT = 300–400 μs (orange) and 100–101 ms (sky blue). Data were measured at pH 5.0 (a) and pH 10.0 (b). The correlated decay curves were calculated by integrating the corresponding two-dimensional emission-delay correlation maps along the 2nd photon axis. Data were normalized at the counts at the microtime of t = 0 (ns). In (b), magnified data are also shown in the inset.

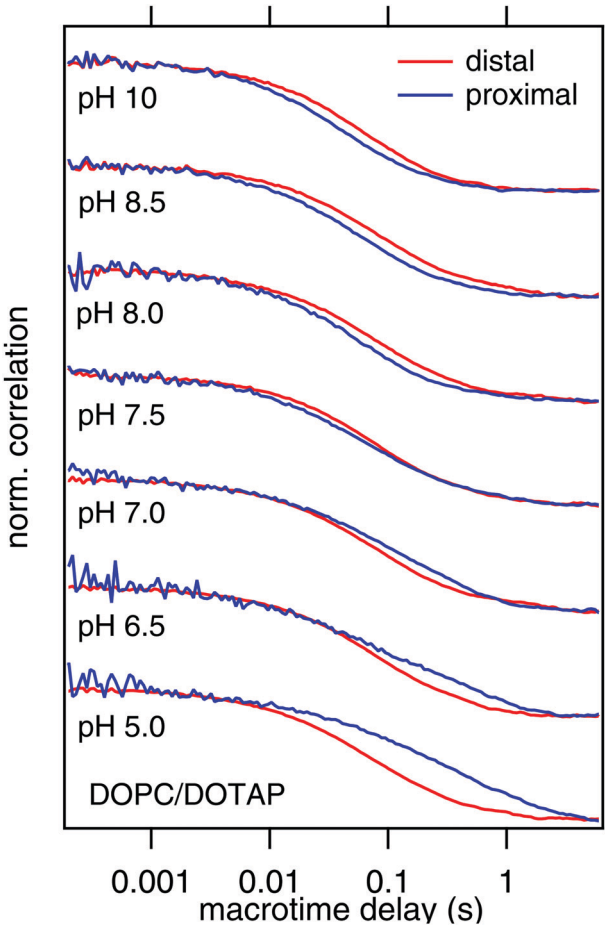

Fig. 5 pH- and leaflet-specific autocorrelation curves of fluorescent lipids in a supported DOPC/DOTAP bilayer. Data were normalized at the correlation amplitudes at the macrotime delay of $\Delta T \sim 1$ ms. Data at different pH were shifted vertically for visual purpose.

even though the lipids in the proximal leaflet interact with a glass support.

To further analyze the leaflet-specific lipid diffusion of the DOPC/DOTAP SLB at high pH, the data are compared with that of the DOPC SLB. Fig. 6 shows the leaflet-specific autocorrelation curves of the DOPC SLB and DOPC/DOTAP SLB measured at pH 10.0. The data are normalized at $\Delta T \sim 1$ ms. The correlation curve of lipids in the proximal leaflet of the DOPC/DOTAP SLB decays faster than other correlation curves. This clearly indicates that the strong electrostatic attraction between the lipid headgroup and a glass surface enhances the lipid diffusion in the proximal leaflet of the SLB.

It is then tempting to analyze the effect of electrostatic repulsion on the leaflet-specific lipid diffusion of SLBs. However, it is known that the electrostatic repulsion between anionic lipids and a glass sometimes makes it difficult to form SLBs.[8,21] Indeed, the formation of stable SLBs when the weight percentage of an anionic lipid, DOPS, exceeds 20% is unsuccessful. Therefore, we performed the following measurements by using the DOPC/DOPS SLB with a DOPC : DOPS weight ratio of 8 : 2.

Fig. 7 shows the leaflet-specific autocorrelation curves of the DOPC/DOPS SLB at various pHs. Representative 2D emission-delay correlation maps and the corresponding independent fluorescence decay curves are shown in Fig. S5 (ESI†), and the filter values used for the calculation and the corresponding cross-correlation curves are shown in Fig. S6 and S7 (ESI†), respectively. Because the carboxyl group of DOPS is reported to be protonated with a pK_a of ~5.5 by the manufacturer, the data were measured with solution pH higher than 6.4. It is also noted that a stable SLB was not formed at pH 10.0 probably due to the strong electrostatic repulsion between the SLB and a glass surface. Thus, the data measured in between pH 6.4 and pH 8.5 are shown. The lipid diffusion in the proximal leaflet of the DOPC/DOPS SLB is slower than that in the distal one in the whole pH regions although the difference is quite small at pH 8.5. This is different from that of the DOPC/DOTAP SLB (Fig. 5). Furthermore, the data at pH 8.5 are also deviated from that of the DOPC SLB where the diffusions of both leaflets were identical at that pH.[35]

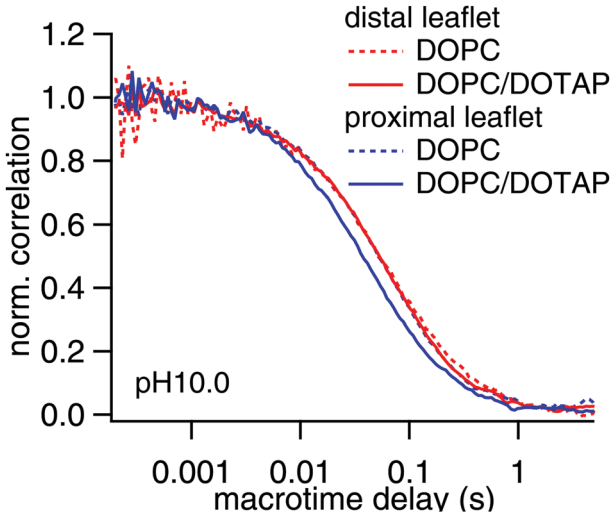

Fig. 6 Comparison of leaflet-specific autocorrelation curves of fluorescent lipids in a supported DOPC/DOTAP bilayer (solid line) and in a supported DOPC bilayer (broken line) measured at pH 10.0. Data of the distal (red) and proximal (blue) leaflets of the supported lipid bilayers are shown. Data were normalized at the correlation amplitudes at the macrotime delay time of $\Delta T \sim 1$ ms.

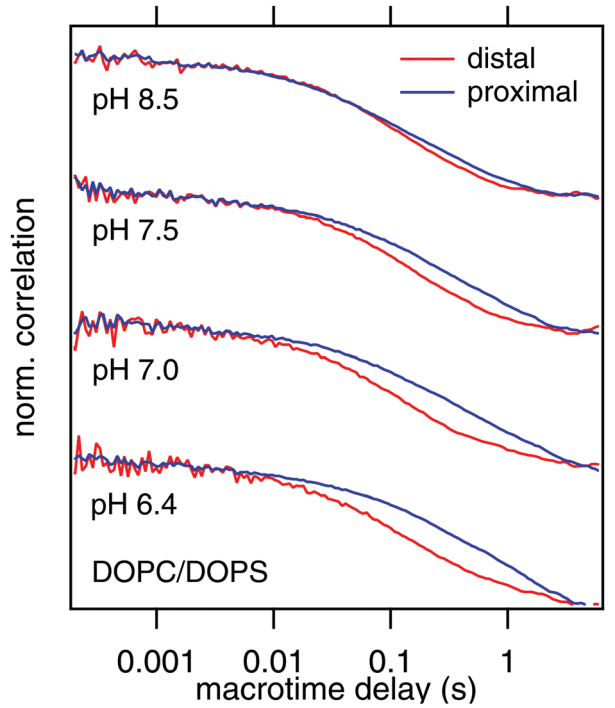

Fig. 7 pH- and leaflet-specific autocorrelation curves of fluorescent lipids in a supported DOPC/DOPS bilayer. Data were normalized at the correlation amplitudes at the macrotime delay of $\Delta T \sim 1$ ms. Data at different pH were shifted vertically for visual purpose.

We previously discussed the diffusion property of the leaflet-specific lipid diffusion by fitting the data with the theoretical model equation.[34] Here, to analyze the pH and lipid-headgroup dependence of the leaflet-specific lipid diffusions in a model-free manner, the data shown in Fig. 5 and 7 are analyzed by calculating the ratio of ΔT (R_{G_0}) between the distal and proximal leaflets, the ΔT of which gives a certain correlation amplitude, G_0:

$$R_{G_0} = \frac{\Delta T_{G_0}^{\text{distal}}}{\Delta T_{G_0}^{\text{proximal}}}. \quad (2)$$

In eqn (2), $\Delta T_{G_0}^{\text{distal}}$ and $\Delta T_{G_0}^{\text{proximal}}$ stand for ΔT that satisfies $G(\Delta T) = G_0$ for the distal and proximal leaflets, respectively. When the lipids in both leaflets show the normal diffusion, R_{G_0} corresponds to the ratio of the diffusion coefficient of the proximal leaflet to that of the distal one. Therefore, the R_{G_0} value is a good indicator of how different the lipid diffusion is in between the proximal and distal leaflets of SLBs.[35]

Fig. 8 shows the pH dependence of R_{G_0} that is calculated with $G_0 = 0.5$ and 0.3. For comparison, the data obtained from the DOPC SLB are also shown.[35] R_{G_0} in the DOPC/DOTAP SLB is larger than 1.0 at high pH, indicating that the diffusion of lipids in the proximal leaflet is faster than that in the distal one as observed in Fig. 5. R_{G_0} decreases at neutral pH and reaches a plateau at acidic pH. The similar pH-dependent trends are observed in the data of the DOPC SLB and DOPC/DOPS SLB although the magnitude of the change is different.

To quantitatively analyze the pH dependence of R_{G_0}, the data of each SLB calculated at two different G_0 (0.5 and 0.3) were fitted together with the following equation:

$$R_{G_0}(\text{pH}) = R_{\text{min}} + \frac{(R_{\text{max}} - R_{\text{min}}) \times 10^{\text{pH}-\text{pH}_{0.5}}}{1 + 10^{\text{pH}-\text{pH}_{0.5}}}. \quad (3)$$

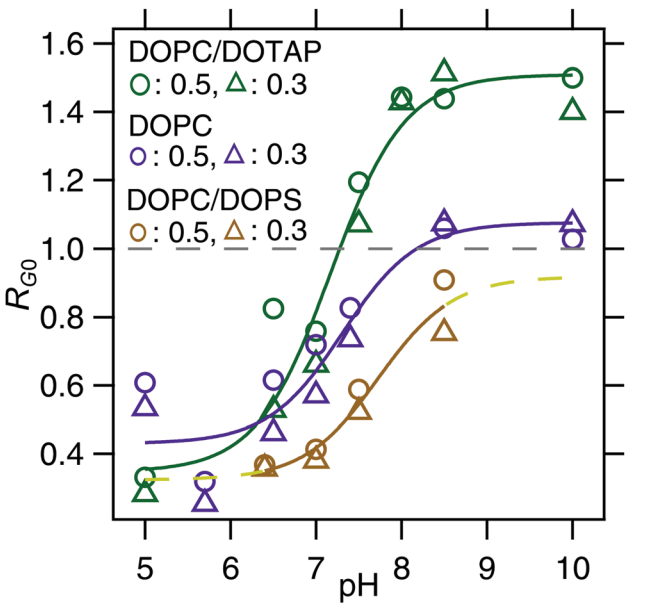

Fig. 8 pH dependence of the ratio of ΔT (R_{G_0}) between the distal and proximal leaflets of supported DOPC/DOTAP (green), DOPC (purple) and DOPC/DOPS (dark yellow) bilayers calculated at the normalized correlation amplitudes of $G_0 = 0.5$ (circle) and 0.3 (triangle). The data of each supported lipid bilayer calculated at the two amplitudes were fitted with eqn (3), and the fitting results are also shown by solid lines with the corresponding colors. The fitting result of a supported DOPC/DOPS bilayer is extrapolated, which is shown with a broken line (yellow).

Table 1 Fitting results

SLB	R_{min}	R_{max}	$pH_{0.5}$
DOPC/DOTAP SLB	0.35	1.5	7.2
DOPC SLB	0.43	1.1	7.3
DOPC/DOPS SLB	0.32	0.92	7.7

where $pH_{0.5}$ is the transition midpoint pH, and R_{min} and R_{max} are the minimum and the maximum R_{G_0}, respectively. All data were well fitted with eqn (3), and the fitting results and obtained parameters are shown in Fig. 8 and Table 1, respectively. Although the value of the DOPC/DOPS SLB is slightly higher, the obtained $pH_{0.5}$ is $\sim$7.5 in all SLBs. Nearly identical $pH_{0.5}$ suggests that the pH-dependent shift in R_{G_0} is not dependent on the lipid composition but is governed by the pH dependence of the surface charge density of a glass surface. Indeed, second harmonic generation studies have shown that the pK_a of surface silanols is $\sim$8,[41,42] in line with this observation. R_{max} is the largest in the DOPC/DOTAP SLB and the smallest in the DOPC/DOPS SLB, where the electrostatic interaction with a glass is attractive and repulsive, respectively. Thus, the results strongly suggest that the magnitude of electrostatic interaction between lipid headgroups and a glass surface is the determinant for the leaflet-specific lipid diffusion in SLBs when the surface charge density of the glass surface is sufficiently large. Lack of the correlation between the net charge of the lipid headgroups and the R_{min} values implies that not only the electrostatic interaction but also other interactions such as van der Waals interactions affect the leaflet-specific lipid diffusion of SLBs at acidic pH.

The enhancement of lipid diffusion induced by the electrostatic attraction between the lipid headgroups and a glass surface has some implication on the microscopic origin of the effect of a solid support on the dynamical properties of SLBs. We previously proposed two possible models for the pH-dependence of the lipid diffusion in the proximal leaflet of SLBs, that is, the lipid packing density model and the solvation layer model.[35] The first model assumes that the lipid packing density of the proximal leaflet depends on the strength of electrostatic interaction between the lipids and a glass surface. On the other hand, the second model assumes that the solvation layer in between a SLB and a glass changes its thickness and/or viscosity depending on the surface charge density of a glass. The observation in this study supports the former one because it is hard to imagine the water structure that enhances the lipid diffusion. Indeed, fluorescence microscopy studies done by Kataoka-Hamai and Higuchi have shown that a small patch of the DOTAP SLB formed by the vesicle fusion of a single giant unilamellar vesicle increases its area by changing the pH of the surrounding solution from acidic to basic, suggesting the decreased packing density at high pH.[12] Furthermore, Ferhan *et al.* utilized a localized surface plasmon resonance sensor to analyze the separation distance between supported lipid bilayers and oxide surfaces.[22] They found that SLB–silica surface proximity, that is, the thickness of the water layer in between the SLB and a silica support is insensitive to the increased content of cationic lipids. Thus, those previous reports as well as the data in this study support the lipid packing density model. Future 2D FLCS studies will further clarify the microscopic origin of the leaflet-specific lipid diffusion on the SLB, which gives the important implication on the lipid dynamics and its relationship with various biological functions of biomembranes.

Conclusions

In this paper, we performed the leaflet-specific lipid diffusion analyses by means of 2D FLCS and FLCS to analyze the effect of lipid–support electrostatic interaction on the lipid diffusion in SLBs. The data clearly showed the correlation between the strength of glass–lipid electrostatic interaction and the lipid diffusion in the proximal leaflet of SLBs. Because a SLB is now widely utilized as a model biomembrane, the results in this study are useful for the future application of SLBs.

Conflicts of interest

There are no conflicts to declare.

Acknowledgements

This work was supported by the Saitama University Tenure Track (SUTT) program and JSPS KAKENHI Grant No. 19H02669.

References

1 B. Alberts, A. Johnson, J. Lewis, D. Morgan, M. Raff, K. Roberts and P. Walter, *Molecular Biology of the Cell*, Garland Science, 6th edn, 2014.
2 J. Soboloff, B. S. Rothberg, M. Madesh and D. L. Gill, *Nat. Rev. Mol. Cell Biol.*, 2012, **13**, 549–565.
3 M. Vassalle, *Experientia*, 1987, **43**, 1135–1140.
4 J. Sjoholm, J. Bergstrand, T. Nilsson, R. Sachl, C. V. Ballmoos, J. Widengren and P. Brzezinski, *Sci. Rep.*, 2017, **7**, 2926.
5 A. Kusumi and K. Suzuki, *Biochim. Biophys. Acta*, 2005, **1746**, 234–251.
6 I. Budin, T. de Rond, Y. Chen, L. J. G. Chan, C. J. Petzold and J. D. Keasling, *Science*, 2018, **362**, 1186–1189.
7 X. L. Cheng and J. C. Smith, *Chem. Rev.*, 2019, **119**, 5849–5880.
8 R. P. Richter, R. Berat and A. R. Brisson, *Langmuir*, 2006, **22**, 3497–3505.
9 E. T. Castellana and P. S. Cremer, *Surf. Sci. Rep.*, 2006, **61**, 429–444.
10 K. L. Hartman, S. Kim, K. Kim and J. M. Nam, *Nanoscale*, 2015, **7**, 66–76.
11 R. Glazier and K. Salaita, *Biochim. Biophys. Acta*, 2017, **1859**, 1465–1482.
12 C. Kataoka-Hamai and M. Higuchi, *J. Phys. Chem. B*, 2014, **118**, 10934–10944.

13 Y. Okamoto, T. Motegi, K. Morita, T. Takagi, H. Amii, T. Kanamori, M. Sonoyama and R. Tero, *Langmuir*, 2016, **32**, 10712–10718.
14 J. S. Allhusen, D. R. Kimball and J. C. Conboy, *J. Phys. Chem. B*, 2016, **120**, 3157–3168.
15 J. S. Allhusen and J. C. Conboy, *Acc. Chem. Res.*, 2017, **50**, 58–65.
16 V. Kiessling, C. Wan and L. K. Tamm, *Biochim. Biophys. Acta*, 2009, **1788**, 64–71.
17 A. Alessandrini and P. Facci, *Soft Matter*, 2014, **10**, 7145–7164.
18 A. K. Shishina, E. A. Kovrigina, A. R. Galiakhmetov, R. Rathore and E. L. Kovrigin, *Biochemistry*, 2018, **57**, 872–881.
19 P. S. Cremer and S. G. Boxer, *J. Phys. Chem. B*, 1999, **103**, 2554–2559.
20 B. Seantier, C. Breffa, O. Felix and G. Decher, *J. Phys. Chem. B*, 2005, **109**, 21755–21765.
21 K. H. Biswas, J. A. Jackman, J. H. Park, J. T. Groves and N. J. Cho, *Langmuir*, 2018, **34**, 1775–1782.
22 A. R. Ferhan, B. Spackova, J. A. Jackman, G. J. Ma, T. N. Sut, J. Homola and N. J. Cho, *Anal. Chem.*, 2018, **90**, 12503–12511.
23 N. J. Cho, J. A. Jackman, M. Liu and C. W. Frank, *Langmuir*, 2011, **27**, 3739–3748.
24 M. P. Goertz, N. Goyal, G. A. Montano and B. C. Bunker, *Langmuir*, 2011, **27**, 5481–5491.
25 S. Stanglmaier, S. Hertrich, K. Fritz, J. F. Moulin, M. Haese-Seiller, J. O. Radler and B. Nickel, *Langmuir*, 2012, **28**, 10818–10821.
26 F. F. Harb and B. Tinland, *Langmuir*, 2013, **29**, 5540–5546.
27 K. Ishii and T. Tahara, *Chem. Phys. Lett.*, 2012, **519–520**, 130–133.
28 K. Ishii and T. Tahara, *J. Phys. Chem. B*, 2013, **117**, 11414–11422.
29 K. Ishii and T. Tahara, *J. Phys. Chem. B*, 2013, **117**, 11423–11432.
30 T. Otosu and S. Yamaguchi, *Molecules*, 2018, **23**, 2972.
31 T. Otosu, K. Ishii and T. Tahara, *Nat. Commun.*, 2015, **6**, 7685.
32 T. Otosu, K. Ishii, H. Oikawa, M. Arai, S. Takahashi and T. Tahara, *J. Phys. Chem. B*, 2017, **121**, 5463–5473.
33 T. Kondo, J. B. Gordon, A. Pinnola, L. Dall'Osto, R. Bassi and G. S. Schlau-Cohen, *Proc. Natl. Acad. Sci. U. S. A.*, 2019, **116**, 11247–11252.
34 T. Otosu and S. Yamaguchi, *J. Phys. Chem. B*, 2018, **122**, 10315–10319.
35 T. Otosu and S. Yamaguchi, *J. Chem. Phys.*, 2019, **151**, 025102.
36 T. Otosu and S. Yamaguchi, *J. Chem. Phys.*, 2017, **147**, 041101.
37 T. Otosu and S. Yamaguchi, *J. Phys. Chem. B*, 2018, **122**, 5758–5764.
38 J. Enderlein and I. Gregor, *Rev. Sci. Instrum.*, 2005, **76**, 033102.
39 P. Kapusta, M. Wahl, A. Benda, M. Hof and J. Enderlein, *J. Fluoresc.*, 2007, **17**, 43–48.
40 A. Ghosh, N. Karedla, J. C. Thiele, I. Gregor and J. Enderlein, *Methods*, 2018, **140**, 32–39.
41 S. W. Ong, X. L. Zhao and K. B. Eisenthal, *Chem. Phys. Lett.*, 1992, **191**, 327–335.
42 M. S. Azam, A. Darlington and J. M. Gibbs-Davis, *J. Phys.: Condens. Matter*, 2014, **26**, 244107.